energies

MDPI

Article

Multi-Criteria Optimal Design for FUEL Cell Hybrid Power Sources

Adriano Ceschia [1], Toufik Azib [1,*], Olivier Bethoux [2] and Francisco Alves [2]

[1] ESTACA'LAB, S2ET Department, ESTACA Engineering School–Paris Sacley, 12 Avenue Paul Delouvrier, 78180 Montigny-le-Bretonneux, France; adriano.ceschia@estaca.fr

[2] GeePs, Group of Electrical Engineering—Paris, UMR CNRS 8507, CentraleSupélec School, University of Paris-Saclay, Sorbonne University, 3 Rue Joliot-Curie, 91192 Gif-sur-Yvette, France; olivier.bethoux@geeps.centralesupelec.fr (O.B.); francisco.alves@geeps.centralesupelec.fr (F.A.)

* Correspondence: toufik.azib@estaca.fr; Tel.: +33-1-76-52-11-03

Abstract: This paper presents the development of a global and integrated sizing approach under different performance indexes applied to fuel cell/battery hybrid power systems. The strong coupling between the hardware sizing process and the system supervision (energy management strategy EMS) makes it hard for the design to consider all the possibilities, and today's methodologies are mostly experience-based approaches that are impervious to technological disruption. With a smart design approach, new technologies are easier to consider, and this approach facilitates the use of new technologies for transport applications with a decision help tool. An automotive application with a hybrid fuel cell (PEMFC)/battery (Li-Ion) is considered to develop this approach. The proposed approach is based on imbricated optimization loops and considers multiple criteria such as the fuel consumption, reliability, and volume of the architecture, in keeping with industry expectations to allow a good trade-off between different performance indexes and explore their design options. This constitutes a low computational time and a very effective support tool that allows limited overconsumption and lifetime reduction for designed architecture in extreme and non-optimal use. We obtain, thanks to this work, a pre-design tool that helps to realize the first conception choice.

Keywords: optimal sizing; reliability assessment; design methodology; hybrid power source; fuel cell/battery; global design methodology; multi-objective optimization

Citation: Ceschia, A.; Azib, T.; Bethoux, O.; Alves, F. Multi-Criteria Optimal Design for FUEL Cell Hybrid Power Sources. *Energies* **2022**, *15*, 3364. https://doi.org/10.3390/en15093364

Academic Editor: Nicu Bizon

Received: 31 March 2022
Accepted: 29 April 2022
Published: 5 May 2022

1. Introduction

Under the impetus of the environmental consideration, the automotive industry is perpetually evolving by targeting the development of alternative energy sources. Electrified mobility seems, in this context, the most promising solution to support and accelerate the transition to sustainable mobility [1,2]. A relevant electrification solution is emerging based on the hybridization concept (hybrid electric vehicle HEV) by using different non-conventional storage and energy sources such as fuel cells, batteries, flywheels, and ultra-capacitors [2,3]. It increases the design and energy management possibilities to face the different constraints of powertrain and new mobility services.

Hybrid architecture, unfortunately, increases the complexity of the drivetrain, involving further additional parameters and constraints, with strong interaction and interdependence between components and supervisory control. This makes many challenges for design engineers to identify the best component sizing and the related EMS (energy management strategy) under many performance indexes to use a suitable engineering methodology [3–6].

In the literature, several works propose various methods to address this issue; two kinds of methodologies emerge in HEV design application: empirical approaches and computational approaches [6]. To deal with the requirements of HEV, computational techniques are required, especially optimization algorithms. The traditional approaches

provide a local solution around the rated operating point. To expand the range of operating points and improve their performance, systematic approaches have been introduced [7,8], based on a sequential process using several individual optimizations or relying on a multi-objective optimization [9–14]. Their feasibility is dependent on the trade-off between formulation complexity, computational time, and exploration capabilities.

New kinds of approaches appear with mixed and combined theories to face the increasing expectations of modern systems. They are organized into three categories: iterative, simultaneous, and imbricated (bi-level) approaches. In [15], an imbricated approach based on a bi-layer Pareto multi-objective optimization problem is formulated to optimally allocate and size an EV parking garage. It tries to make trade-offs to maximize the profits of the EV parking garage investor as well as minimize the losses and voltage deviations for the distribution system operator. In [16], an iterative approach using an uncertain bilevel programming model is proposed for optimal energy dispatching of an integrated energy system. It considers the multi-energy complementarity among multiple decision-makers for the economy of the system operation. In [17], a general overview of simultaneous strategies for dynamic optimization problems is suggested, including the design of control systems. They have clear advantages by allowing the rapid determination of accurate solution profiles with fewer time steps than with sequential methods. For hybrid power sources, interaction problems in the design process (sizing and control designs) and the relevance and performance of simultaneous and imbricated approaches have been shown by many works in the literature [17–20].

For simultaneous paradigms, the process realizes both optimizations (sizing and control) using the same formulation. With this approach, the performances are better due to the ability to realize parallel calculations, but it creates more complexity for interdependence problems (formulation, computation time). On the other hand, imbricated ones (coupled optimization) allow the possibility of making a simple and performant implementation. We already suggested a new imbricated approach for hybrid system design with large search space ability [18]. This proposed methodology simultaneously designs and tunes the component sizing and energy management by optimizing several parameters (power, capacity, and response time of the sources) according to the specifications. Two imbricated loops are used to implement this approach, the particle swarm optimization (PSO) for system sizing and the Pontryagin optimal control algorithm (PMP Pontryagin's Minimum Principle) for EMS. With this approach, we can quickly obtain an optimal solution with good accuracy and robustness, considering the large search space and the convergence ability of the global methodology.

Furthermore, in modern vehicle applications, and specifically in hybrid and electric vehicles (HEV/EV), the design process should consider various performance indexes beyond the energetic consideration; reliability and sizing space (volume) are the most important for transport applications. Actual design methodologies integrate these factors in a post-design process [21–23], which is not optimal, considering the complexity and the presence of multiple attributes. The reliability is currently solved by using oversized design and limitations in the EMS (degraded modes monitoring). For example, an EMS based on a demand response program and a hydrogen storage system is introduced in [23]. The system degradation is conducted by reducing peak demand and by limiting the response of the sources. This solution is not accurate to improve the system reliability; it is helpless for the sizing consideration. In addition, it induces energy overconsumption, which significantly reduces the system efficiency under real stochastic use.

Considering recent studies [24–27], the availability and reliability of fuel cell/battery hybrid systems have been addressed by introducing an appropriate EMS. For example, a conscious EMS algorithm based on Model Predictive Control (MPC), which aims to minimize the battery degradation to extend its lifetime, is proposed in [24]. Another study [25] proposes a review of degradation modeling methods of lithium-ion batteries and PEM fuel cells, and the possibility of integrating them into health-conscious energy management is discussed. They conclude, however, that the system reliability is highly

dependent on the considered sizing. Therefore, the reliability and sizing consideration should be studied in the early stage of the design process.

Motivated by the gap in the literature and to increase the relevance of our nested design approach, a reliability assessment process only for the battery has been introduced, showing the impact of the reliability consideration on design choices regarding the energetic performance index [28]. In previous work, the reliability impact was considered in the post-processing step to sort all the proposed solutions of the optimization regarding the battery reliability. Previous work highlights the need for a multi-objective optimization technique to generate the trade-off between different performance indexes (reliability and size) and to explore their design options by including in the optimization process the impact of the considered indexes. We also considered in this new approach the impact of the fuel cell reliability during the optimization process. We can understand easily, with this approach, the correlations that exist between sizing, energy management, and the reliability of the architecture. It helps design engineers to set up the best hybridization rate and to include various constraints in the early design stages.

In this study, we consider the same use case with a fuel cell-battery hybrid vehicle (FCHV), which is one of the most promising solutions for hybrid electric vehicles (HEV) developed in the latest years [5,21,23,29]. It allows combining the advantages of each technology to improve the vehicle efficiency and reliability since it enhances the system capability with lifetime enhancement, high power, and high energy densities. The fuel cell (FC) is a proton exchange membrane fuel cell (PEMFC), and the battery (BAT) is a lithium-ion battery (Li-Ion). To consider lifetime estimation under use conditions, a Whöler damage model is implemented. It uses a linear extrapolation (extracted from experimental data) to obtain a reliable BAT and FC state of health (SOH) to allow simple and easy integration into the global methodology approach, considering computing time constraints. Regarding the size of the final architecture, the estimation of sizing space (volume) is based on Ragon's diagram to ensure the easy implementation of this consideration. Introducing this setup allows a better space exploration to make a set of optimal solutions while containing the complexity and computation time. This paper aims to present a new paradigm in transport architecture designing, considering different challenges in the transport industry.

This paper is organized as follows. Section 2 presents the optimal design methodology and the studied use case (FCHEV). Section 3 introduces additional performance indexes about the reliability process and the volume estimation through the FC SOH, the BAT SOH, and the implementation of the global methodology. Section 4 presents the simulation results and discussion about the global process. The last section discusses the conclusion and perspectives for our work.

2. Optimal Design Approach Based on Imbricated Architecture

2.1. Use Case

To illustrate the performance of our new design approach, we used a parallel hybrid fuel cell/battery source with a DC/DC converter for each source, which is one of the most promising solutions for HEV. This architecture is commonly used in the literature for its numerous freedom degrees that allow a wide range of EMS optimization [30]. Figure 1 presents this architecture, with the FC considered as the main energy source and the battery as the auxiliary power/energy source. The city car Renault ZOE was used for the vehicle specifications model (weight, surface, etc.) to evaluate the power cycle of the FCEV demand according to different normalized speed cycles (WLTC, US 06, US Highway, etc.).

2.2. Principle of Design Approach

Using the mono-objective methodology presented in previous work [28], a multi-objective approach that considers different performance indexes (energy-consuming, reliability, volume) was developed. This approach aims to propose to design engineers a decision support tool to simultaneously consider many objectives and study the trade-offs between them.

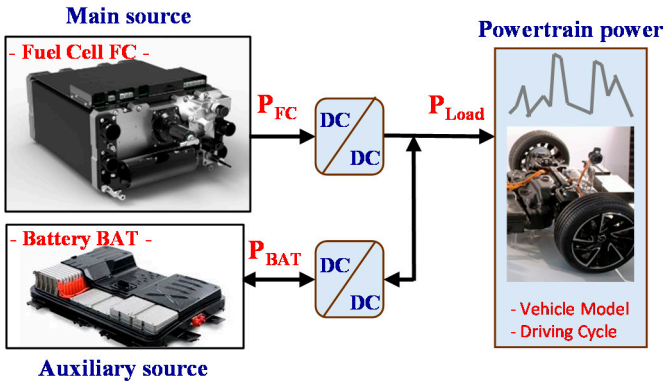

Figure 1. Parallel hybrid FC/BAT power source architecture [28].

The proposed global design approach is based on two nested optimizations, which are relevant to support the interdependence between the sizing and the energy management in power architecture design. This involves identifying values of the key parameters influencing system design considering various performance indexes to meet the requirements. Figure 2 represents this new global methodology approach.

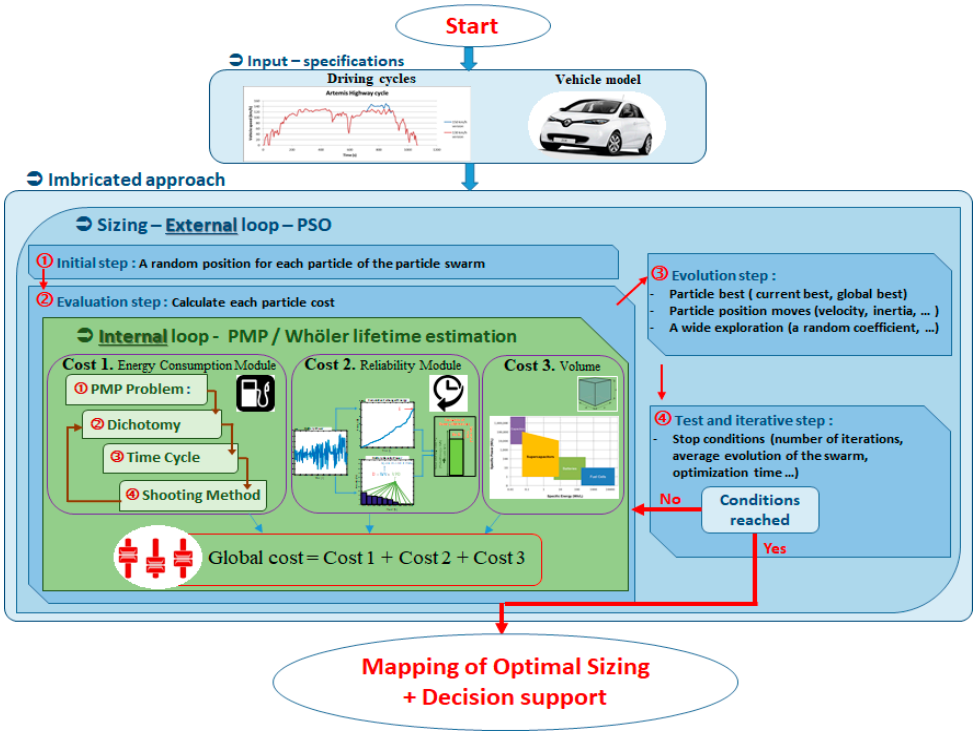

Figure 2. Workflow implementing the proposed nested decision support tool.

External optimization: This step realizes the optimization of the main sizing parameters. It assesses each solution based on internal optimization with different index estimations. When the stop conditions are reached, the optimization stop and best solution are presented.

Internal optimization: For each tested architecture, a multi-objective optimization is performed with different performance indexes (energy consumption, reliability, volume) and associated cost weighting.

Both optimizations are constrained by the parameter's limits but also the behavior's limits to respect the architecture's integrity and specifications. With this approach, the ponderation between each performance index is available according to the requirements.

The methodology produces a swarm of the optimal solution for each possible ponderation, which constitutes an effective decision support tool.

3. Imbricated Optimization Loops

3.1. External Optimization Loop

Based on the most relevant techniques in the literature, the PSO technique was selected to search for the best system parameters to optimize the main sizing parameters of the architecture: FC power (P_{FC}), BAT power (P_{BAT}), and BAT capacity (C_{BAT}).

This technique is particularly adapted to address large design spaces, including the advantages of implementation simplicity, good convergence, and short computing time [31,32]. The PSO algorithm is based on swarm intelligence (social behavior of birds), which makes a search mechanism based on the movement of a population. It uses both randomness and information sharing between particles to identify the best position (i.e., optimal variable values). The search space is defined by optimization variables considering the specifications. Figure 2 represents the PSO design process of the sizing optimization, whose development is detailed in [7].

3.2. Internal Optimization Loop

This loop makes a multi-objective optimization using three modules: energy, reliability, and volume, to evaluate each sizing architecture.

3.2.1. Energy Consumption Module

For energy consideration, the EMS is required to minimize the total FC consumption by managing, in real-time, the power split between FC and BAT. For this purpose, the PMP is a very powerful technique and provides a good accuracy/speed of calculation ratio compared to other EMS optimizations such as dynamic programming (DP) [33–35]. It allows identifying a unique optimal trajectory for energy saving by minimizing a Hamilton function. The optimization process (Figure 2) is detailed in [7].

3.2.2. Reliability Module

Based on previous works [28] dedicated to BAT reliability, this study makes an extension of the reliability assessment of the FC/BAT hybrid power source.

Battery Reliability

By its nature, the BAT can face the transient power demand, unlike the FC, which will affect its durability, specifically in automotive applications [26]. The BAT degradation appears through capacity loss and internal resistance increase, which results in loss of energy capacity and power availability. The State of health (*SOH*) is the index that represents the BAT degradation/reliability defined in Equation (1) [36,37]:

$$SOH = \frac{C_{BAT,\,C}}{C_{BAT,\,Init}} \quad (1)$$

where *SOH* is BAT State of Health, $C_{BAT,C}$ and $C_{BAT,Init}$ are the current and initial battery capacities.

Lithium-ion BAT SOH decreases with use conditions and time storage. BAT aging is a complex and multi-factor process (electrical, thermal, humidity, mechanical, and chemical parameters). However, the thermal aspect is predominant [36–41] through the calendar aging effect and the cycling effect [37,42]. The calendar effect [36,40] mainly depends on the storage conditions, ambient temperature, and state of charge (*SOC*).

The cycling aging is impacted by the battery usage [36,40,43], such as the number of cycles, the depth of discharge (*DOD*), the battery temperature, and the average demanded power. In [36–48], aging and SOH are considered according to calendar and cycling to obtain a theoretical or empirical model; in our case, only cycling aging will be considered. These approaches are complex and require a time-consuming process. Moreover, the test cycles are not representative of a real automotive driving use.

We showed in [28] that the effect of each aging parameter could be modeled by a quasi-linear relationship. The main aging effect selected is the deep of discharge (DOD) and the normalized current of the cycle (normalized by the battery capacity C_{BAT}, also called rated current). We applied the Whöler approach describing the relation between stress factor level and the number of cycles to failure to create a mathematical model based on literature test data results.

The end-of-life (*EOL*) of the BAT is considered when the loss of battery capacity reaches 20% of the initial capacity [49]. With this approach, we could obtain the following empirical model shown in Equations (2) and (3) and Figures 3 and 4.

$$\begin{cases} SOH_{DOD}(\%) = 100 - \frac{DOD(\%)}{\gamma} \cdot N_{Cycle,DOD} \\ N_{Cycle,DOD} = \alpha \cdot DOD(\%) + \beta \end{cases} \quad (2)$$

$$\begin{cases} SOH_{Ic}(\%) = 100 - \frac{C_{rate}}{\delta} \cdot N_{Cycle,Ic} \\ N_{Cycle,Ic} = \rho \cdot C_{rate} + \sigma \end{cases} \quad (3)$$

where SOH_{DOD} and SOH_{Ic} are the state of health as a function of *DOD* and rated current, respectively. N_{Cycle}, *DOD*, and $N_{Cycle,Ic}$ are the number of cycles according to a *DOD* level and a normalized current, respectively. C_{rate} is the normalized charge/discharge current. α, β, γ, δ, ρ, and σ are fitting parameters.

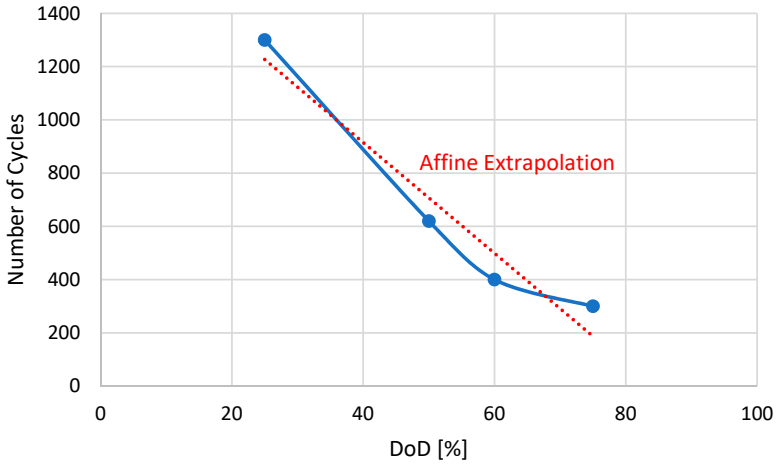

Figure 3. A linear trend extrapolation of BAT *SOH* according to *DOD* variation [28].

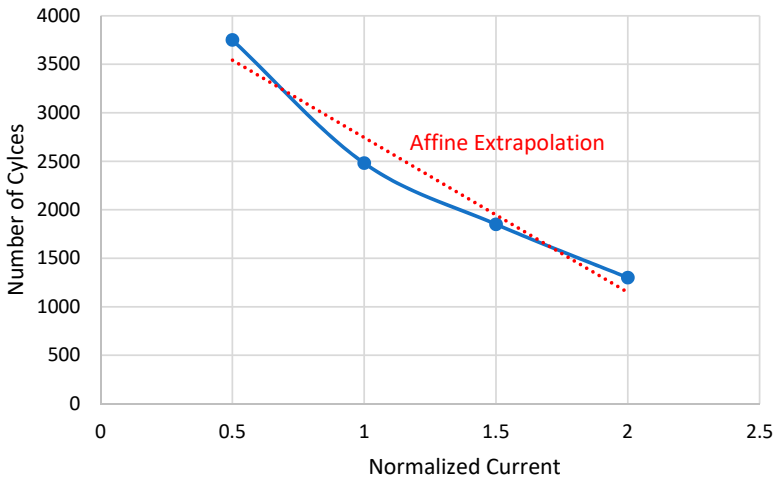

Figure 4. A linear trend extrapolation of BAT *SOH* according to normalized current variation [28].

With this model, we obtain an estimation of the BAT *SOH* considering several cycles, which is dependent on the cycle specification; we translated it into exchanged energy to "normalize" the cycle.

The final reliability assessment is estimating the residual lifetime by weighting the cumulative energy exchanged according to the power density of the cycle. Figure 5 shows each step of the proposed reliability assessment module.

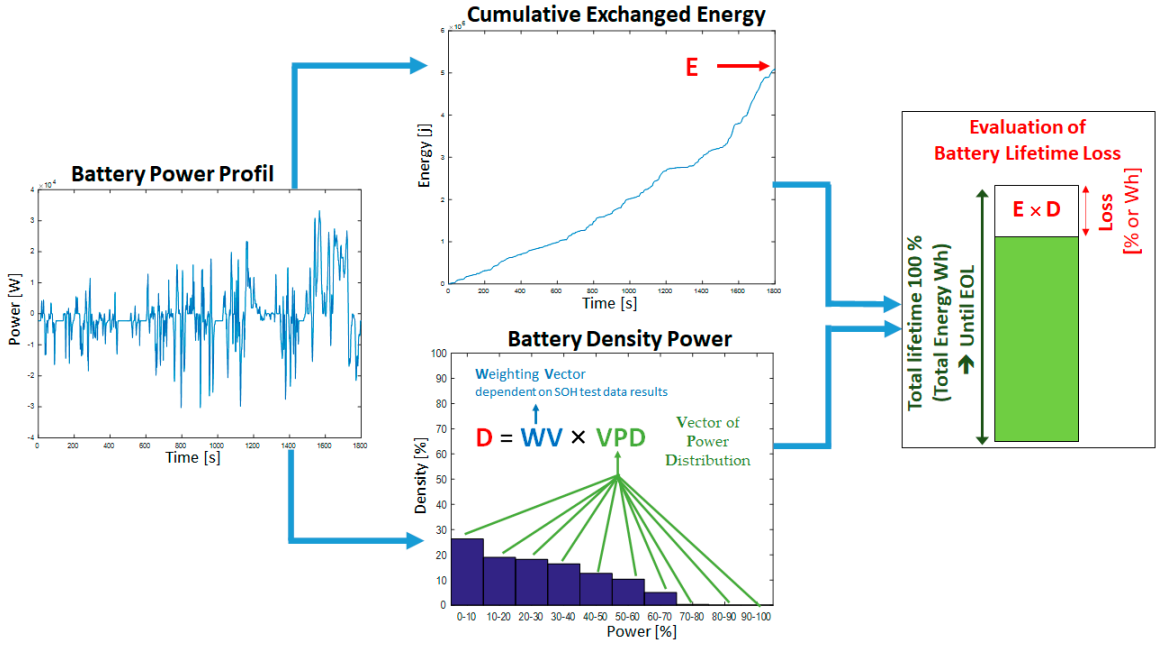

Figure 5. Battery reliability assessment module [28].

This approach is very flexible, using available data from the literature, which is adapted to different BAT technologies. It considers a global reliability assessment based on the average evolution of aging factors until EOL is reached. This leads to fast results with a low complexity, which is suitable for a global design methodology. The following section presents the process for the FC reliability estimation module.

Fuel Cell Reliability

The FC is commonly dedicated to supplying the main power, in a hybrid architecture, due to its bad performance in transient behaviors. Its performance depends mainly on membrane management (gas pressure and velocity, thermal and water management, etc.) which is a big challenge for its lifetime and operational availability [36].

The FC degradation appears through losses of power availability and can be evaluated by the state of health (*SOH*) defined in Equation (4) [50]:

$$SOH = \frac{P_{FC,\,C}}{P_{FC,\,Init}} \tag{4}$$

where *SOH* is FC state of health, $P_{FC,C}$, and $P_{FC,Init}$ are the current and initial FC power.

The EOL of FC in automobile applications is commonly determined by an SOH of around 80% to ensure safe operating conditions.

The PEMFC aging is a complex and multi-factor process (electrical, thermal, humidity, mechanical, and chemical parameters). However, these processes can be summarized through the four kinds of use [51,52] presented in Figure 6. In new energy management strategies dedicated to the hybrid pour sources for transport applications, the FC system is equipped with a start-up procedure (cold start, thermal management, system shutdown, stuck draining process, etc.), which significantly limits the impact of the start, stop, and

idling phases [51]. In these conditions, only the high power and transient phase have been considered in this work.

For the first mechanism [51–55], the experimental studies based on accelerated results shown in Figure 7 reveal the evolution of the SOH for different power supplied at a constant rate.

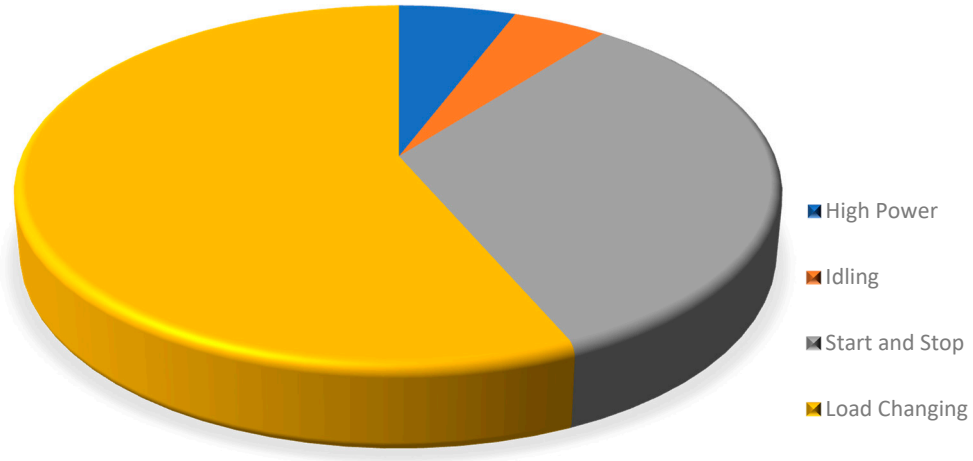

Figure 6. Aging processes of FC (PEMFC) [55].

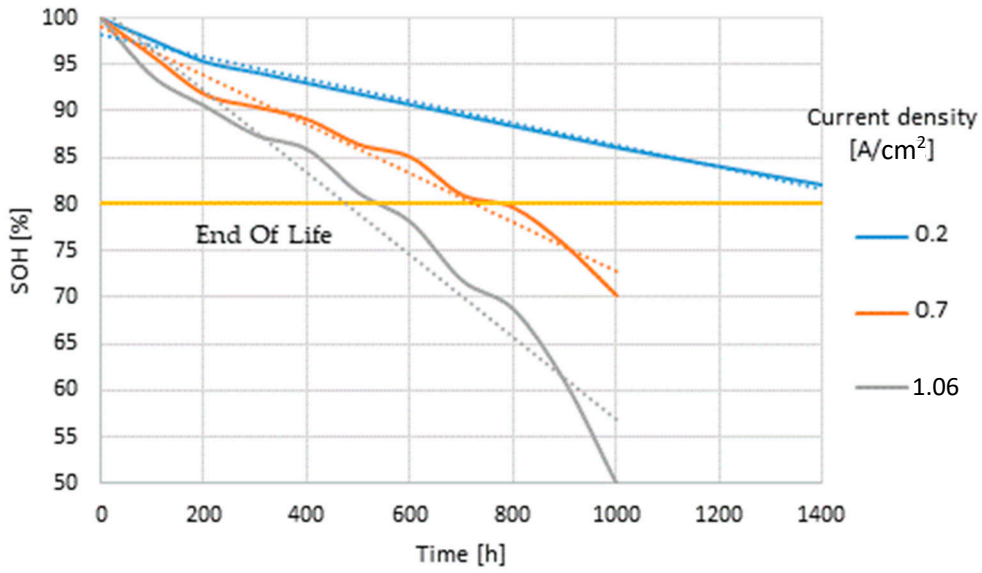

Figure 7. Power rate—FC aging behavior.

We can see that for a constant power supplied by the FC, the SOH evolves almost linearly in a proportional way considering the rated power. We use the same approach presented in the previous section, based on the Whöler approach, to create a qualitative lifetime assessment. It considers the aging behavior of linear PEMFC regarding the power rate (Figure 8).

The second aging process is led by load change amplitude in the FC use; we proceeded, in the same way, looking for experimental accelerated results (Figure 9) of SOH estimation according to load change amplitude [51–55].

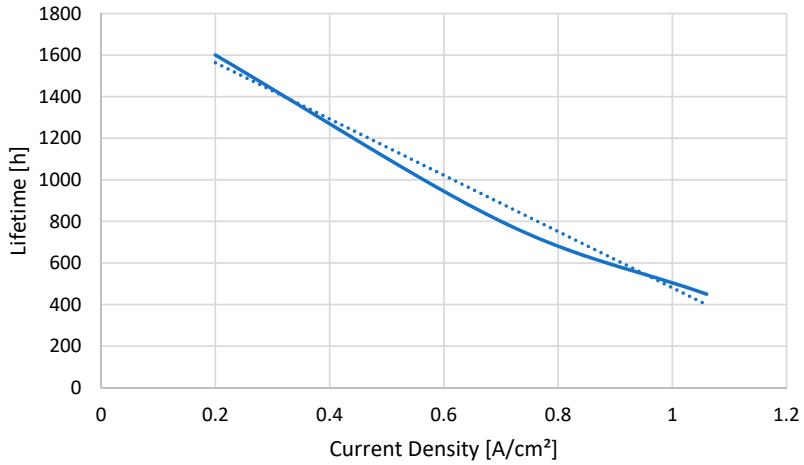

Figure 8. Current Density—FC aging model.

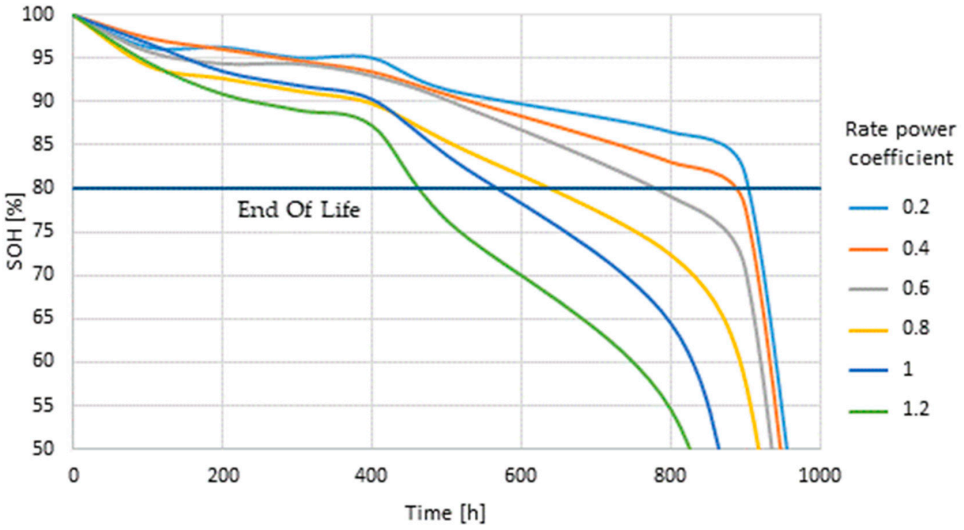

Figure 9. Load change amplitude—FC aging behavior.

As for the BAT, the behavior of the aging process, considering the load changes amplitude, can be linearized using a Whöler curve to consider the load change effect on the aging process (Figure 10).

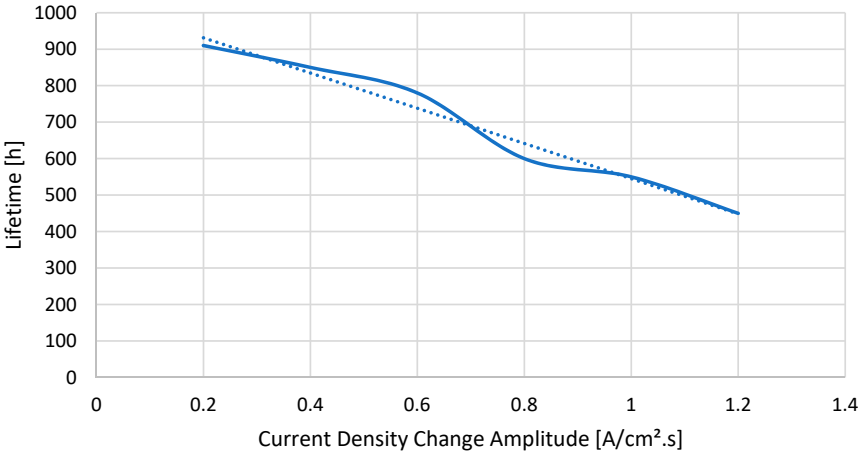

Figure 10. Load change amplitude—FC aging model.

Both aging models (power rating (Figure 8) and load change amplitude (Figure 9)) can be summarized in the mathematic Equations (5) and (6),

$$\begin{cases} SOH_{PR}(\%) = a - b \times PR\left(A/cm^2\right) \times T(h) \\ T_{PR}(h) = c \times PR + d \end{cases} \quad (5)$$

$$\begin{cases} SOH_{LC}(\%) = e - f \times LC\left(A/cm^2.s\right) \times T(h) \\ T_{LC}(h) = g \times LC + h \end{cases} \quad (6)$$

with: SOH_{PR} and SOH_{LC} the state of health considering power rate and load change; T, T_{PR}, and T_{LC} the time, time under power rate, and time under load change; PR and LC the power rate and load change; and a, b, c, d, e, f, g, h some coefficients to determine short experimental testing on the considered FC.

The FC lifetime assessment module uses a mathematic formulation based on the power rate and load change aging models and some accounting of the time spent in each aging situation [54]. It allows a simple methodology, compatible with the BAT reliability estimation, for assessing the effect of the energy management strategy on the FC lifetime (Figure 11). This model can be presented in the following mathematic formulation (Equations (7)–(9)):

$$T\ (h) = \frac{\Delta\ P\ (\%)}{k \times (C_1 \times P_1(\%.h^{-1}) + C_2 \times P_2(\%.h^{-1}))} \quad (7)$$

$$\begin{cases} Counter_{Power\ rate}(s) = \sum X_i(P_i) \\ C_1 = Counter_{Power\ rate}/3600 \end{cases} \quad (8)$$

$$\begin{cases} Counter_{Load\ Change}(s) = \sum Y_i \\ C_2 = Counter_{Load\ Change}/3600 \end{cases} \quad (9)$$

with T, the estimated lifetime; ΔP, the accepted FC power loss; k, a correcting coefficient to calibrate the model; C_1 and C_2, the power rate and load changer counter; P_1 and P_2, the coefficient extracted from the power rate and load change aging model previously presented.

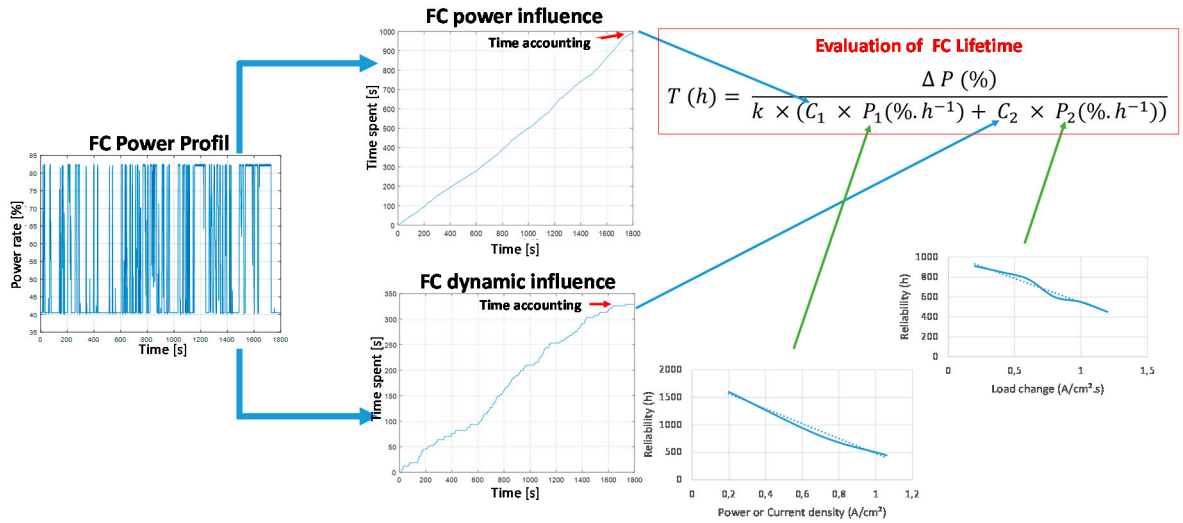

Figure 11. Fuel Cell reliability assessment module.

In the counting process, we realize a cumulative addition of each second of the cycle during which the FC is used at the considered condition (Figure 11). For the power rate, each second (Xi) of the cycle pondered by the power rate (Pi) is counted (1 s is counted as 1 when the FC is at 100% of power and counted as 0.5 s when the FC is at 50% of power). For

the load changes, each second (Yi) is counted when the FC realizes a load change and is not counted when the FC is at constant load.

The result of this approach gives us a lifetime estimation of the FC in the current use conditions; this estimation is in hours of use. To be suitable with our global methodology and BAT lifetime estimation, we convert this lifetime to Joule (J) by considering the average consumed FC energy on the tested cycle.

Global Reliability

The global reliability is generated considering the two previously presented modules (BAT reliability and FC reliability). The global cost is performed by weighted addition with the two results. The ponderation is currently chosen with a 50:50 ratio but can be modified by the final user of the global methodology to suit its application.

3.2.3. Volume Module

The volume estimation is based on the sizing value proposed by the PSO algorithm. At each optimization step, several possible solutions are available, each consisting of a possible combination value for each sizing parameter (power of the FC, BAT capacity, etc.). Using a RAGONE plot (Figure 12) to compare the performance of various energy devices, the corresponding volume can be deduced for each source following its technology [56].

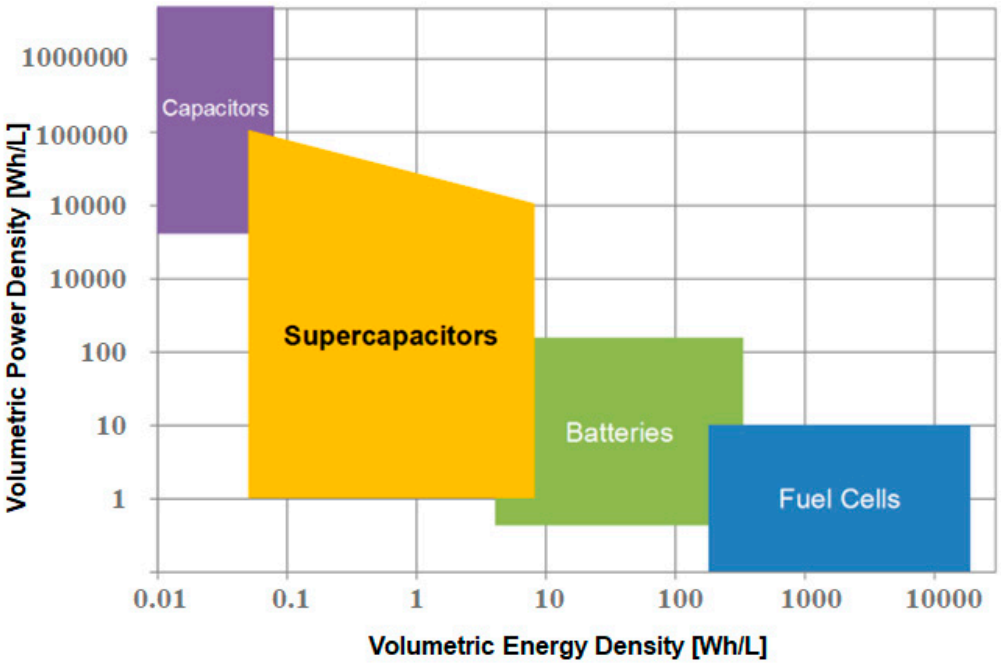

Figure 12. Ragone plot [57].

The global volume of the architecture is thus given in Equation (10):

$$Index_{Vol} = Z_1 \times P_{Spec}FC \times P_{FC} + Z_2 \times E_{Spec}Bat \times C_{Bat} + V_{acc} \quad (10)$$

with $Index_{Vol}$, the estimated volume of the architecture; $P_{Spec}FC$ and $E_{Spec}Bat$, the specific power of *FC* technologies and the specific energy of the Li-Ion Bat technologies; P_{FC} and C_{Bat}, the sized power of the *FC* and the size capacity of the BAT; V_{acc}, a constant volume to consider the accessory architecture volume (converter for example); and Z_1, Z_2, coefficients to tune the ponderation between each volume in the global volume estimation.

4. Results and Analysis

The proposed decision support tool was tested by an extensive simulation using the MATLAB/SIMULINK environment (R2018a, MathWorks, Natick, MA, USA); the hardware was a core i7 at 3.2 GHz with 16Go of RAM. The study was carried out with three performance indexes (energy consumption, reliability, volume), for which the results involve three-dimension mapping. It is realized for a ponderation from 0% to 100% with a step of 1% for three different cycles WLTC, US Highway, US 06.

The objective is to observe the dominance and influence of each criterion on the variation of real driving conditions to make available and relevant indicators for a designer to guide this final choice.

The main parameters used in our simulations are illustrated in Table 1. Note that FC/BAT models (PEMFC, Li-Ion) and associated parameters are presented in detail in a previous study [18].

Table 1. Support tool parameters [28].

Parameter	Value	Parameter	Value
Particle number and Iteration	50, 500	Vehicle mass (kg)	1428
Values to design	P_{FC}, C_{BAT}	Air density (kg·m^{-3})	1.2
Search field: P_{FC}, C_{BAT}	1–50 kW and 1–10 kWh	Friction coefficient	0.012
Fuel cell, battery models	PEMFC static, Li-Ion model	Aerodynamic coefficient	0.29
SOC_{Min}, SOC_{Max}	15%, 90%	Front surface area (m^2)	2.69
γ, α, β	1400, −20, 1700	δ, ρ, σ	125, −1600, 4400

The results of complete space solutions are presented in Figures 13–15 with a three-dimension mapping (up left) and two-dimension projections for three cycles: the WLTC, the US Highway, and the US 06.

The results exhibit a coherent behavior with three asymptotic surfaces that represent the best results of each objective (energy, reliability, volume) and a space solution curve, making the trade-off solutions to identify interesting design candidates. This is due to the antagonism and strong dependency between performance indexes. The volume tends to undersize the architecture while the energy consumption orients the sizing to enhance the performance.

Another important issue related to the driving conditions, with a concentration of sizing architecture towards the lower consumption limit under low dynamic cycles (US highway), while they are more distributed for dynamic cycles (WLTC). It can be seen that the cycle had a moderate impact on the distribution of the results about the other criteria. This can be explained by the strong influence of energy management and the approach's ability to find trade-off solutions depending on driving conditions.

Furthermore, the maps contain some discontinuities related to the computing capacity. Indeed, the accuracy of the design mapping was reduced to keep an acceptable time of calculation (around 48 h to 72 h for two objectives and 1 to 2 weeks for three objectives).

In addition, it was easy to find indicators relating to the system behavior for each objective. From the WLTC data, we extracted some remarkable values to highlight the usefulness of this approach (Table 2).

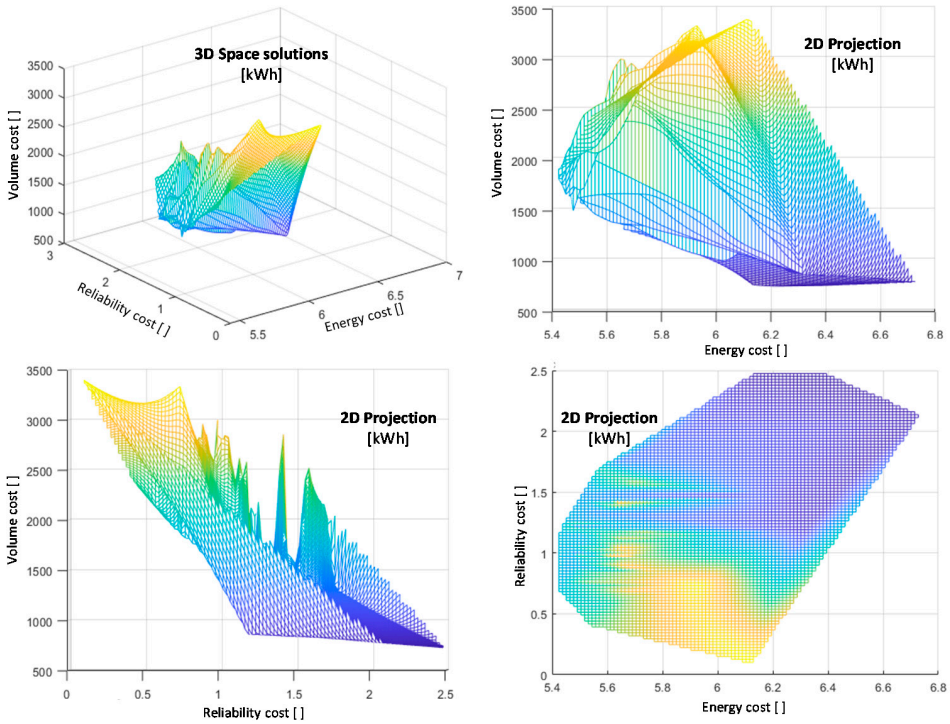

Figure 13. Design mapping on WLTC Cycle.

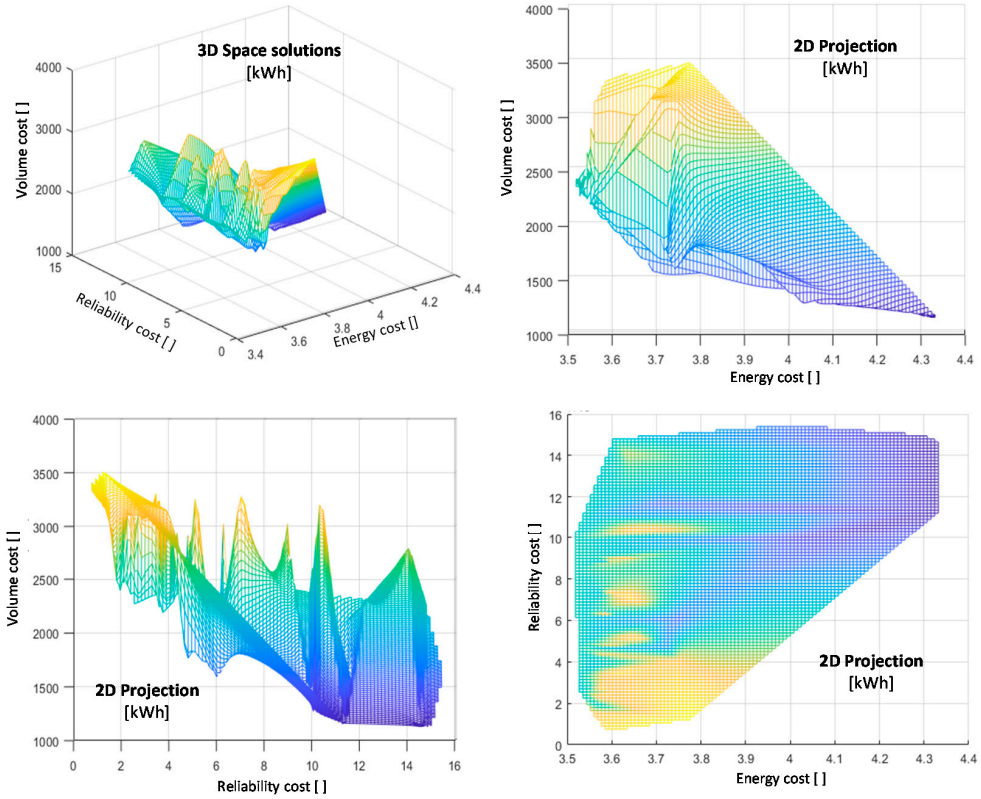

Figure 14. Design mapping on US Highway Cycle.

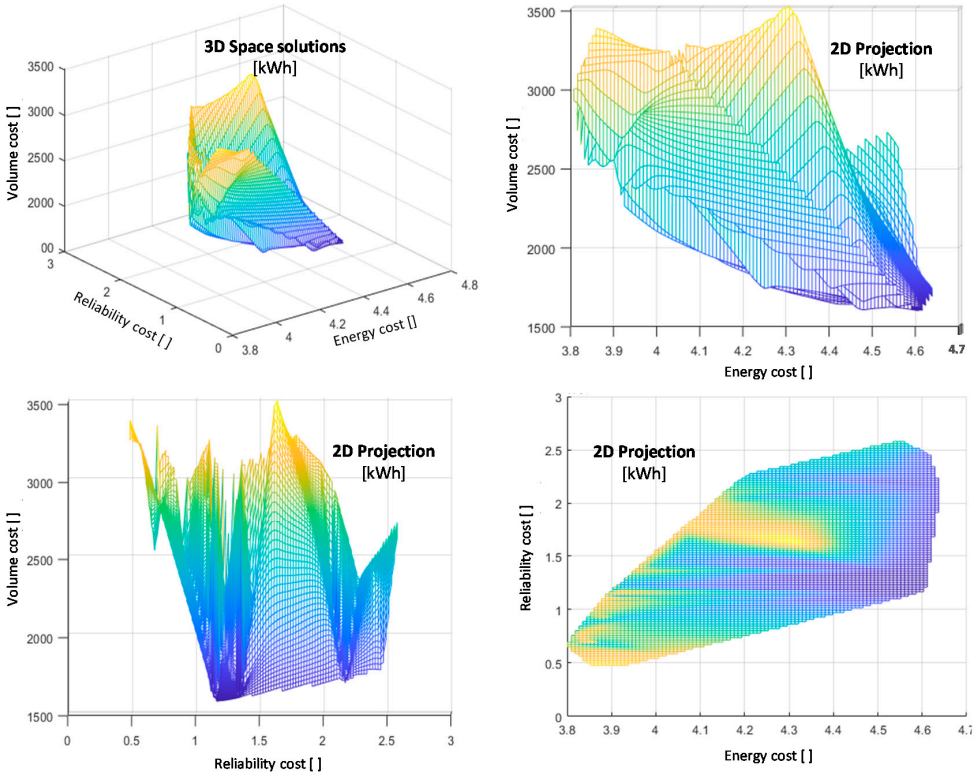

Figure 15. Design mapping on US 06 Cycle.

Table 2. WLTC design values.

	Energy Consumption	Reliability	Volume	FC Power	BAT Capacity
Best Consumption Solution	5.4 kWh → 0.71 kg H2/100 km	~10,300 Cycles	~190 L	16.9 kW	9.9 kWh
Best Reliability Solution	6.1 kWh → 0.90 kg H2/100 km	~20,800 Cycles	~265 L	32.67 kW	9.44 kWh
Best Volume Solution	6.2 kWh → 0.92 kg H2/100 km	~8400 Cycles	~95 L	14.0 kW	2.5 kWh
Trade-Off Solution	5.8 kWh → 0.76 kg H2/100 km	~13,900 Cycles	~205 L	24 kW	7.9 kWh

These results show the relevance and interest of this approach regarding the complexity and variety of the possible solutions by considering several objectives simultaneously. Indeed, the proposed methodology is performed to provide the appropriate decision for the system designers in the search for the trade-off solutions available between these conflicting objectives in reduced time and costs.

First, the volumes proposed are two to three times higher than the optimal solution (better volume). In this last case, the overconsumption generated was around 30%, and the lifetime was considerably reduced compared to the best reliability solution. Finally, a compromise solution was proposed, which allows keeping the lifetime and volume targets with moderate overconsumption, around 10%. These results show the relevance of considering additional performance indexes at the same level in the pre-design phase showing their early impact on design choices (optimal size and the related energy management strategy). This constitutes a very effective support tool to help design engineers to include various constraints in the early design stages.

5. Conclusions

This work shows the relevance of considering several performance indexes in the design process under different driving cycles and operating conditions. In hybrid power sources, the interaction between system sizing and control parameters is a crucial point that should be considered in the design process; the proposed multi-objective approach based on nested optimization loops aims to facilitate this interaction to find an optimal solution in reduced time and costs. It leads to a smart design methodology avoiding complexity and saving computing time by considering several industrial performance indexes to improve the quality of the global optimal design. This constitutes a very effective support tool to considerably help design engineers to integrate more constraints and make trade-offs between available solutions in the early design stages to face the increasing expectations of the hybrid electric drivetrains.

This approach is modular and can be scaled to other applications; this flexible new paradigm allows us to consider the main industrial challenges not only as constraints but also as a performance index to support the optimal design of such systems.

Based on this approach, future work will consider the integration of this methodology in real use with a real-time energy management module.

Author Contributions: Conceptualization: A.C., T.A., O.B. and F.A.; methodology: A.C. and T.A.; additional performance indexes: T.A. and O.B.; writing—original draft preparation: A.C. and T.A.; writing—review and editing: T.A., O.B. and F.A.; supervision: T.A, O.B. and F.A. All authors have read and agreed to the published version of the manuscript.

Funding: This research received no external funding.

Conflicts of Interest: The authors declare no conflict of interest.

Abbreviations

EOL	End-of-Life
EMS	Energy Management Strategy
HEV	Hybrid Electric Vehicle
PSO	Particle Swarm Optimization
PMP	Pontryagin's Minimum Principle
EV	Electrical Vehicle
FCHV	Fuel Cell Hybrid Vehicle
PEMFC	Proton Exchange Membrane Fuel Cell
SOH	State of Health
WLTC	Worldwide Harmonized Light Vehicles Test Cycles
US Highway	Highway United States Test Cycle
US06	Supplemental United States Test Cycle
VPD	Vector of Power Distribution
WV	Weighting Vector
D	Degradation degree
L_{oss}	Lifetime loss
SOH	State of Health
DOD	Depth of Discharge
Z_1, Z_2	Weighting coefficient
$P_{FC/C/init}$	Fuel cell power, Current, Initial, (W)
P_{BAT}	Battery power, (W)
$C_{BAT/C/Init}$	Battery capacity, Current, Initial, (Ah)
$SOC_{Max/Min}$	Battery state of charge, Maximum, Minimum, (%)
P_{Load}	Power demand, (W)
$C_{BAT,C}$, $C_{BAT,Init}$	Current and initial battery capacity, (Wh)
SOC, SOC_0	Current and initial State Of Charge, (%)
i_{BAT}	Battery current, (A)
SOH_{DOD}	State of health as a function of DOD
SOH_{Ic}	State of health as a function of rated current.

$N_{Cycle,DOD}$	Number of cycles according to a DOD level
$N_{Cycle,Ic}$	Number of cycles according to a ratted current.
C_{rate}	Charging/discharge current, (A)
$\alpha, \beta, \gamma, \delta, \rho, \sigma$	BAT Fitting parameters.
E_{BAT}	Battery cumulated energy, (*J* or Wh)
$N_{Cycle,Init}$	Initial number of cycles.
T, T_{PR}, T_{LC}	Estimating lifetime, Time under Power Rate, Time under Load Change, (s, h)
SOH_{PR}	State of health considering Power Rate
SOH_{LC}	State of health considering Load Change
a, b, c, d, e, f, g, h	FC Fitting parameters.
PR, LC	Power Rate, Load Change
ΔP	Accepted FC power loss
k	Correcting coefficient
P_1, P_2	Coefficient from aging models
C_1, C_2	Power rate counter, Load Changer counter
$P_{SpecFC}, E_{SpecBat}$	FC Specific Power, BAT Specific Energy
$Index_{Vol}$	Estimated volume
V_{acc}	A constant volume to consider the accessories

References

1. Muneer, T.; Kolhe, M.; Doyle, A. *Electric Vehicles: Prospects and Challenges*; Elsevier: New York, NY, USA, 2017; ISBN 978-0-12-803021-9.
2. Croce, A.I.; Musolino, G.; Rindone, C.; Vitetta, A. Traffic and Energy Consumption Modelling of Electric Vehicles: Parameter Updating from Floating and Probe Vehicle Data. *Energies* **2022**, *15*, 82. [CrossRef]
3. Do, T.C.; Truong, H.V.A.; Dao, H.V.; Ho, C.M.; To, X.D.; Dang, T.D.; Ahn, K.K. Energy Management Strategy of a PEM Fuel Cell Excavator with a Supercapacitor/Battery Hybrid Power Source. *Energies* **2019**, *12*, 4362. [CrossRef]
4. Yao, G.; Du, C.; Ge, Q.; Jiang, H.; Wang, Y.; Ait-Ahmed, M.; Moreau, L. Traffic-Condition-Prediction-Based HMA-FIS Energy-Management Strategy for Fuel-Cell Electric Vehicles. *Energies* **2019**, *12*, 4426. [CrossRef]
5. Fu, Z.; Li, Z.; Si, P.; Tao, F. A hierarchical energy management strategy for fuel cell/battery/supercapacitor hybrid electric vehicles. *Int. J. Hydrog. Energy* **2019**, *44*, 22146–22159. [CrossRef]
6. Egan, P.; Cagan, J. Human and Computational Approaches for Design Problem-Solving. In *Experimental Design Research*; Cash, P., Stanković, T., Štorga, M., Eds.; Springer International Publishing: Cham, Switzerland, 2016; pp. 187–205. ISBN 978-3-319-33779-1.
7. Serpi, A.; Porru, M. Modelling and Design of Real-Time Energy Management Systems for Fuel Cell/Battery Electric Vehicles. *Energies* **2019**, *12*, 4260. [CrossRef]
8. Silvas, E.E.; Hofman, T.T.; Murgovski, N.N.; Etman, L.F.P.; Steinbuch, M.M. Review of Optimization Strategies for System-Level Design in Hybrid Electric Vehicles. *IEEE Trans. Veh. Technol.* **2017**, *66*, 57–70. [CrossRef]
9. Yang, Y.; Shang, Z.; Chen, Y.; Chen, Y. Multi-Objective Particle Swarm Optimization Algorithm for Multi-Step Electric Load Forecasting. *Energies* **2020**, *13*, 532. [CrossRef]
10. Hu, B.; Wang, N.; Yu, Z.; Cao, Y.; Yang, D.; Sun, L. Optimal Operation of Multiple Energy System Based on Multi-Objective Theory and Grey Theory. *Energies* **2022**, *15*, 68. [CrossRef]
11. Zhou, X.; Qin, D.; Hu, J. Multi-objective optimization design and performance evaluation for plug-in hybrid electric vehicle powertrains. *Appl. Energy* **2017**, *208*, 1608–1625. [CrossRef]
12. Nandi, A.K.; Chakraborty, D.; Vaz, W. Design of a comfortable optimal driving strategy for electric vehicles using multi-objective optimization. *J. Power Sources* **2015**, *283*, 1–18. [CrossRef]
13. Gharibi, M.; Askarzadeh, A. Size and power exchange optimization of a grid-connected diesel generator-photovoltaic-fuel cell hybrid energy system considering reliability, cost and renewability. *Int. J. Hydrog. Energy* **2019**, *44*, 25428–25441. [CrossRef]
14. Chen, H.; Yang, C.; Deng, K.; Zhou, N.; Wu, H. Multi-objective optimization of the hybrid wind/solar/fuel cell distributed generation system using Hammersley Sequence Sampling. *Int. J. Hydrog. Energy* **2017**, *42*, 7836–7846. [CrossRef]
15. Faddel, S.G.; Elsayed, A.T.; Mohammed, O.A. Bilayer Multi-Objective Optimal Allocation and Sizing of Electric Vehicle Parking Garage. *IEEE Trans. Ind. Appl.* **2018**, *54*, 1992–2001. [CrossRef]
16. Song, X.; Lin, H.; De, G.; Li, H.; Fu, X.; Tan, Z. An Energy Optimal Dispatching Model of an Integrated Energy System Based on Uncertain Bilevel Programming. *Energies* **2020**, *13*, 477. [CrossRef]
17. Biegler, L.T. An overview of simultaneous strategies for dynamic optimization. *Chem. Eng. Process. Process Intensif.* **2007**, *46*, 1043–1053. [CrossRef]
18. Ceschia, A.; Azib, T.; Bethoux, O.; Alves, F. Optimal design methodology for sizing a fuel cell/battery hybrid power source. *J. Power Energy* **2021**, *235*, 1277–1286. [CrossRef]
19. Tran, D.-D.; Vafaeipour, M.; El Baghdadi, M.; Barrero, R.; Van Mierlo, J.; Hegazy, O. Thorough state-of-the-art analysis of electric and hybrid vehicle powertrains: Topologies and integrated energy management strategies. *Renew. Sustain. Energy Rev.* **2020**, *119*, 109596. [CrossRef]

20. Herber, D.R.; Allison, J.T. Nested and Simultaneous Solution Strategies for General Combined Plant and Control Design Problems. *J. Mech. Des.* **2019**, *141*, 11402–11413. [CrossRef]
21. Wang, Y.; Moura, S.J.; Advani, S.G.; Prasad, A.K. Optimization of powerplant component size on board a fuel cell/battery hybrid bus for fuel economy and system durability. *Int. J. Hydrog. Energy* **2019**, *44*, 18283–18292. [CrossRef]
22. Song, Z.; Zhang, X.; Li, J.; Hofmann, H.; Ouyang, M.; Du, J. Component sizing optimization of plug-in hybrid electric vehicles with the hybrid energy storage system. *Energy* **2018**, *144*, 393–403. [CrossRef]
23. Maghami, M.R.; Hassani, R.; Gomes, C.; Hizam, H.; Othman, M.L.; Behmanesh, M. Hybrid energy management with respect to a hydrogen energy system and demand response. *Int. J. Hydrog. Energy* **2020**, *45*, 1499–1509. [CrossRef]
24. Sellali, M.; Ravey, A.; Betka, A.; Kouzou, A.; Benbouzid, M.; Djerdir, A.; Kennel, R.; Abdelrahem, M. Multi-Objective Optimization-Based Health-Conscious Predictive Energy Management Strategy for Fuel Cell Hybrid Electric Vehicles. *Energies* **2022**, *15*, 1318. [CrossRef]
25. Yue, M.; Jemei, S.; Gouriveau, R.; Zerhouni, N. Review on health-conscious energy management strategies for fuel cell hybrid electric vehicles: Degradation models and strategies. *Int. J. Hydrog. Energy* **2019**, *44*, 6844–6861. [CrossRef]
26. Tao, L.; Ma, J.; Cheng, Y.; Noktehdan, A.; Chong, J.; Lu, C. A review of stochastic battery models and health management. *Renew. Sustain. Energy Rev.* **2017**, *80*, 716–732. [CrossRef]
27. Martinez-Laserna, E.; Gandiaga, I.; Sarasketa-Zabala, E.; Badeda, J.; Stroe, D.I.; Swierczynski, M.; Goikoetxea, A. Battery second life: Hype, hope or reality? A critical review of the state of the art. *Renew. Sustain. Energy Rev.* **2018**, *93*, 701–718. [CrossRef]
28. Ceschia, A.; Azib, T.; Bethoux, O.; Alves, F. Optimal Sizing of Fuel Cell Hybrid Power Sources with Reliability Consideration. *Energies* **2020**, *13*, 3510. [CrossRef]
29. Jayakumar, A.; Chalmers, A.; Lie, T.T. Review of prospects for adoption of fuel cell electric vehicles in New Zealand. *IET Electr. Syst. Transp.* **2017**, *7*, 259–266. [CrossRef]
30. Azib, T.; Bethoux, O.; Remy, G.; Marchand, C.; Berthelot, E. An Innovative Control Strategy of a Single Converter for Hybrid Fuel Cell/Supercapacitor Power Source. *IEEE Trans. Ind. Electron.* **2010**, *57*, 4024–4031. [CrossRef]
31. Guo, X.; Yan, X.; Chen, Z.; Meng, Z. A Novel Closed-Loop System for Vehicle Speed Prediction Based on APSO LSSVM and BP NN. *Energies* **2022**, *15*, 21. [CrossRef]
32. Yang, R.; Yuan, Y.; Ying, R.; Shen, B.; Long, T. A Novel Energy Management Strategy for a Ship's Hybrid Solar Energy Generation System Using a Particle Swarm Optimization Algorithm. *Energies* **2020**, *13*, 1380. [CrossRef]
33. Yuan, Z.; Teng, L.; Fengchun, S.; Peng, H. Comparative Study of Dynamic Programming and Pontryagin's Minimum Principle on Energy Management for a Parallel Hybrid Electric Vehicle. *Energies* **2013**, *6*, 2305–2318. [CrossRef]
34. Liu, J.; Feng, L.; Li, Z. The Optimal Road Grade Design for Minimizing Ground Vehicle Energy Consumption. *Energies* **2017**, *10*, 700. [CrossRef]
35. Liu, C.; Liu, L. Optimal power source sizing of fuel cell hybrid vehicles based on Pontryagin's minimum principle. *Int. J. Hydrog. Energy* **2015**, *40*, 8454–8464. [CrossRef]
36. Wilberforce, T.; Khatib, F.; Ijaodola, O.; Ogungbemi, E.; El-Hassan, Z.; Durrant, A.; Thompson, J.; Olabi, A. Numerical modelling and CFD simulation of a polymer electrolyte membrane (PEM) fuel cell flow channel using an open pore cellular foam material. *Sci. Total Environ.* **2019**, *678*, 728–740. [CrossRef]
37. Thompson, A.W. Economic implications of lithium ion battery degradation for Vehicle-to-Grid (V2X) services. *J. Power Sources* **2018**, *396*, 691–709. [CrossRef]
38. Babin, A.; Rizoug, N.; Mesbahi, T.; Boscher, D.; Hamdoun, Z.; Larouci, C. Total Cost of Ownership Improvement of Commercial Electric Vehicles Using Battery Sizing and Intelligent Charge Method. *IEEE Trans. Ind. Appl.* **2018**, *54*, 1691–1700. [CrossRef]
39. Maher, K.; Yazami, R. A study of lithium ion batteries cycle aging by thermodynamics techniques. *J. Power Sources* **2014**, *247*, 527–533. [CrossRef]
40. Maheshwari, A.; Heck, M.; Santarelli, M. Cycle aging studies of lithium nickel manganese cobalt oxide-based batteries using electrochemical impedance spectroscopy. *Electrochim. Acta* **2018**, *273*, 335–348. [CrossRef]
41. Tang, X.; Zou, C.; Yao, K.; Chen, G.; Liu, B.; He, Z.; Gao, F. A fast estimation algorithm for lithium-ion battery state of health. *J. Power Sources* **2018**, *396*, 453–458. [CrossRef]
42. Ma, S.; Jiang, M.; Tao, P.; Song, C.; Wu, J.; Wang, J.; Deng, T.; Shang, W. Temperature effect and thermal impact in lithium-ion batteries: A review. *Prog. Nat. Sci. Mater Int.* **2018**, *28*, 653–666. [CrossRef]
43. Pelletier, S.; Jabali, O.; Laporte, G.; Veneroni, M. Battery degradation and behaviour for electric vehicles: Review and numerical analyses of several models. *Transp. Res. Part B Methodol.* **2017**, *103*, 158–187. [CrossRef]
44. Han, X.; Ouyang, M.; Lu, L.; Li, J. A comparative study of commercial lithium ion battery cycle life in electric vehicle: Capacity loss estimation. *J. Power Sources* **2014**, *268*, 658–669. [CrossRef]
45. Martel, F.; Dubé, Y.; Kelouwani, S.; Jaguemont, J.; Agbossou, K. Long-term assessment of economic plug-in hybrid electric vehicle battery lifetime degradation management through near optimal fuel cell load sharing. *J. Power Sources* **2016**, *318*, 270–282. [CrossRef]
46. Leng, F.; Tan, C.M.; Pecht, M. Effect of Temperature on the Aging rate of Li Ion Battery Operating above Room Temperature. *Sci. Rep.* **2015**, *5*, 12967. [CrossRef]
47. Zou, Y.; Hu, X.; Ma, H.; Li, S. Combined State of Charge and State of Health estimation over lithium-ion battery cell cycle lifespan for electric vehicles. *J. Power Sources* **2015**, *273*, 793–803. [CrossRef]
48. Ecker, M.; Nieto, N.; Käbitz, S.; Schmalstieg, J.; Blanke, H.; Warnecke, A.; Sauer, D.U. Calendar and cycle life study of Li(NiMnCo)O2-based 18650 lithium-ion batteries. *J. Power Sources* **2014**, *248*, 839–851. [CrossRef]

49. Quinard, H.; Redondo-Iglesias, E.; Pelissier, S.; Venet, P. Fast Electrical Characterizations of High-Energy Second Life Lithium-Ion Batteries for Embedded and Stationary Applications. *Batteries* **2019**, *5*, 33. [CrossRef]
50. Zhang, D.; Baraldi, P.; Cadet, C.; Yousfi-Steiner, N.; Bérenguer, C.; Zio, E. An ensemble of models for integrating dependent sources of information for the prognosis of the remaining useful life of Proton Exchange Membrane Fuel Cells. *Mech. Syst. Signal Process.* **2019**, *124*, 479–501. [CrossRef]
51. Durst, J.; Lamibrac, A.; Charlot, F.; Dillet, J.; Castanheira, L.F.; Maranzana, G.; Dubau, L.; Maillard, F.; Chatenet, M.; Lottin, O. Degradation heterogeneities induced by repetitive start/stop events in proton exchange membrane fuel cell: Inlet vs. outlet and channel vs. land. *Appl. Catal. B Environ.* **2013**, *138–139*, 416–426. [CrossRef]
52. LaConti, A.B.; Hamdan, M.; McDonald, R.C. Mechanisms of Membrane Degradation. In *Handbook of Fuel Cells*; John Willey & Sons: Newton, MA, USA, 2010. [CrossRef]
53. Morando, S.; Jemei, S.; Hissel, D.; Gouriveau, R.; Zerhouni, N. Proton exchange membrane fuel cell ageing forecasting algorithm based on Echo State Network. *Int. J. Hydrog. Energy* **2017**, *42*, 1472–1480. [CrossRef]
54. Zhao, J.; Li, X. A review of polymer electrolyte membrane fuel cell durability for vehicular applications: Degradation modes and experimental techniques. *Energy Convers. Manag.* **2019**, *199*, 112022. [CrossRef]
55. Pei, P.; Chang, Q.; Tang, T. A quick evaluating method for automotive fuel cell lifetime. *Int. J. Hydrog. Energy* **2008**, *33*, 3829–3836. [CrossRef]
56. Sang, C.L.; Woo Young, J. Analogical Understanding of the Ragone plot and a New Categorization of Energy Devices. *Energy Procedia* **2016**, *88*, 526–530. [CrossRef]
57. CAP-XX Ltd. Energy Storage Technologies. 6 April 2015. Available online: https://www.cap-xx.com/resource/energy-storage-technologies/ (accessed on 24 April 2022).